Chinese Chemical Letters 34 (2023) 108306

Contents lists available at ScienceDirect

Chinese Chemical Letters

journal homepage: www.elsevier.com/locate/cclet

Two-dimensional g-C_3N_4 nanosheets-based photo-catalysts for typical sustainable processes

Xiaodong Zhao[a], Qian Liu[b], Xiaolei Li[a,*], Huiming Ji[a], Zhurui Shen[b,*]

[a] Key Laboratory of Advanced Ceramics and Machining Technology, Ministry of Education, School of Materials Science and Engineering, Tianjin University, Tianjin 300072, China
[b] School of Materials Science and Engineering, Nankai University, Tianjin 300350, China

ARTICLE INFO

Article history:
Received 29 October 2022
Revised 6 February 2023
Accepted 5 March 2023
Available online 11 March 2023

Keywords:
Graphitic carbon nitride (g-C_3N_4)
nanosheets
Exfoliation approaches
Hetero-junction
Z-scheme mechanism
Photo-catalytic applications

ABSTRACT

Graphitic carbon nitride (g-C_3N_4) has been widely studied as a visible light responsive photocatalyst in recent years, due to its facile synthesis, low cost, high stability, and appropriate bandgap/band positions. In this review, we firstly introduce and compare various exfoliation approaches of bulk g-C_3N_4 into ultrathin g-C_3N_4 nanosheets. Then, many modification strategies of g-C_3N_4 nanosheets are also reviewed, including heterojunction construction, doping, defect control, and structure design. Thereafter, the charge transfer mechanism in g-C_3N_4 nanosheets based heterojunctions is present, *e.g.*, Z-scheme, S-scheme and other forms. Besides, the photocatalytic applications of g-C_3N_4 nanosheets based photocatalysts are summarized including environmental remediation, energy generation and storage, organic synthesis, and disinfection. This review ends with a summary and some perspectives on the challenges and new directions in exploring g-C_3N_4 nanosheets-based photocatalysts.

1. Introduction

All the time severe environment pollution and latent source crisis have drawn increasingly attention towards solar energy utilization by reason of the merits including environmentally friendly and inexhaustible supply. As a consequence, semiconductor photocatalysts are considered to be a potential strategies for pollutant elimination and clean energy acquisition. Research on semiconductor photo-catalysis was initiated in 1972 with the application towards photo-chemical hydrogen generation by TiO_2 electrodes [1], however, the large bandwidth leaded to low spectral utilization rate, numerous approaches have been applied to absorb added solar irradiation, improving the photo-catalytic ability subsequently [2–6]. Besides, many other semiconductors such as ZnO, WO_3, SnO_2 [7–16] have also been identified as potential photo-catalysts. However, the low sunlight absorption as well as poor separation ability of photo-generated charges still block the development of photo-catalytic materials towards higher catalytic activity [17–19], a huge number of research articles, including coupling with heterogeneous semiconductors, element doping, and defect controlling, has been published on the modification of photo-catalysts for better performance [20–27].

Recently, graphite-like carbon nitride (g-C_3N_4) has drawn plenty of study on account of simple preparation, low price, high tolerance against temperature, acid or alkali solutions, and narrow band-gap with appropriate band position (*ca.* −1.3 eV and *ca.* +1.4 eV) [28–30], which can be widely used in water splitting, CO_2 reduction, dye-stuff decomposition, disinfection and so on [31–39]. The history of g-C_3N_4 for photo-catalysis can be traced back to 2009 [40], Wang *et al.* firstly utilized this tri-*s*-triazines material for photo-catalytic water splitting. The g-C_3N_4 nanosheets was synthesized by Niu *et al.* for the first time in 2012 [41], the bulk g-C_3N_4 was thinned to 2 nm thick *via* thermal treatment, the photo-catalytic activities have been remarkably improved due to increased specific area, the enhanced charge transport ability and the improved lifetime of photo-induced charges compared with bulk g-C_3N_4. Nevertheless, the original g-C_3N_4 is limited in photocatalytic reaction because of the disadvantages including poor sunlight spectral utilization and quick annihilation rate of photo-generated charges [42–46], in recent years, many attempts, such as construction of hetero-junctions, doping, dye sensitization, and structure design, have been made in towards modification of g-C_3N_4 nanosheets [47–58]. Among those methods, hetero-structures construction towards g-C_3N_4 enhanced the photo-catalytic capacity due to the effective separation performance as well as fast migrate ability of photo-induced charges. Meanwhile, the carries transfer mechanism in hetero-junctions has been studied by the-

* Corresponding authors.
E-mail addresses: lxlei@tju.edu.cn (X. Li), shenzhurui@nankai.edu.cn (Z. Shen).

https://doi.org/10.1016/j.cclet.2023.108306
1001-8417/

oretical calculation and characterization for the deeply understanding about the improvement of photo-catalytic performance [59–64].

This review concentrates on numerous research towards the exfoliation methods, modification strategies, mechanistic understanding and adhibition of g-C_3N_4 nanosheets-based nanocomposites. Primarily, the main preparation approaches of ultra-thin g-C_3N_4 nanosheets are presented and compared. Secondly, several methods for elevating the performance of g-C_3N_4 nanosheets, such as construction of hetero-junctions, elements doping, defect controlling, and building nanostructures, are discussed. Next, the type-II system, Z-scheme as well as S-scheme mechanism were presented, demonstrating the charge migrate process in g-C_3N_4 nanosheets-based hetero-junctions. Another section of this review summarizes the photo-catalytic adhibition of g-C_3N_4 nanocomposites applying to pollution decomposition, hydrogen production, nitrogen fixation, disinfection and so on. Finally, this paper gives some conclusions and further perspectives about above mentioned researches, in turn, promoting more effective application towards this photo-catalytic material.

2. Exfoliation of g-C_3N_4 into 2D nanosheets

g-C_3N_4 is a layered material which consists of the multilayer two-dimensional conjugated structures formed *via* tri-*s*-triazines cells [65], the acting force between different layers is weaker than the interlayer binding force [66,67]. Since two-dimensional nanosheets have many excellent advantages, including huge specific area, ultrahigh electron mobility, as well as plentiful surface reactive sites [68–70], it is highly rational to thinning bulk layered g-C_3N_4 to attain less layers nanosheets for much superior photo-catalytic performance.

The thinning for multilayer matter was applied in clay materials, which could spontaneously swell and delaminate with the destroy of interlayer interaction in water [71,72]. In 2004, K. Novoselov and co-workers [73] attained graphene with many intriguing properties by the mechanical exfoliation towards graphite, since then, great efforts have been made to exfoliate layered materials into nanosheets [74–78]. Because of the similarities between graphite and g-C_3N_4, the exfoliation of the latter into nanosheets has been widely studied [79–84], the synthetic approaches which have been established included the temperature, ultrasonic and chemical exfoliation.

2.1. Thermal oxidation exfoliation

Niu *et al.* prepared thinned g-C_3N_4 nanosheets for the first time [41]. Based on the knowledge the force between layers including van der Waals' force as well as the hydrogen bond are not strong enough to withstand thermal energy, leading to the separation between different layers [85], as a consequence, a decrease of thickness to the desired nanoscale happened, the g-C_3N_4 nanosheets with the approximate 2 nm thick (6∼7 layers) was obtained after thermal exfoliation from bulk materials in air at high temperature (Fig. 1a). The as-prepared nanosheets exhibited huge specific area (306 m^2/g), enhanced charge mobility, and prolonged life-span for photo-excited charges, the photo-catalytic activities have been remarkably enhanced as a consequence. The preparation of nanosheets *via* temperature treatment depended on many factors, such as etching time, temperature, precursor masses, and atmosphere [86–90]. Graphene-like g-C_3N_4 nanosheets with promoting photo-catalytic capacity was synthesized by Dong and his researchers [91] *via* a thermal exfoliation approach under different temperatures from 450 °C to 550 °C, with the elevation of temperature, the thickness of resultant nanosheets gradually decreased, the surface area increased at the meantime. Until now, the thermal oxidation strategy for g-C_3N_4 nanosheets with improved photo-catalytic ability has been widely applied because of its low-cost and easy operation [92–99].

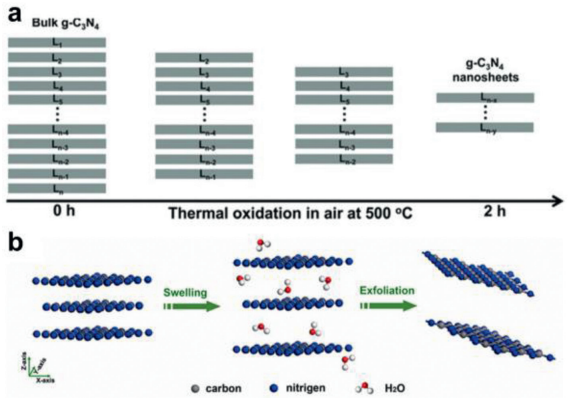

Fig. 1. (a) Schematic of the formation process of the g-C_3N_4 nanosheets by thermal oxidation etching of bulk g-C_3N_4 at 500 °C in air. Reproduced with permission [41]. Copyright 2012, Wiley. (b) Schematic illustration of the liquid-exfoliation process from bulk g-C_3N_4 to ultra-thin nanosheets. Reproduced with permission [100]. Copyright 2012, American Chemical Society.

2.2. Ultrasonic exfoliation

Liquid exfoliation of layered materials *via* ultrasonic process is considered to be a effective way for preparing two-dimensional nanosheets [75]. Synthesizing ultra-thin g-C_3N_4 nanosheets through ultrasonic treatment route from bulk material in solvent is environmentally friendly and can result in a relatively high product yield compared to thermal oxidation etching approach [79]. During the exfoliation process, solvent molecules would intercalate into layered materials, resulting in enlarging of lamellar spacing as well as damage of van der Waals force among different layers, at the meantime, the ultrasonic-produced bubbles would gradually oscillate and crack, leading to the liquid jets which could shear the layered materials into ultra-thin nanosheets. It is known that the similar surface energy between the bulk g-C_3N_4 as well as reagent molecules would bring efficient exfoliation for high-yield g-C_3N_4 nanosheets [74], besides, the polarity solvent could be more effective for intercalation and swelling due to the presence of dangling hydrogens among multilayer g-C_3N_4 material. Zhang and co-workers [100] firstly delaminated bulk g-C_3N_4 in water to form nanosheets with an approximate 2.5 nm thick, layered g-C_3N_4 was swelled and exfoliated after the intercalation of water molecules under ultrasonic conditions (Fig. 1b). To date, ultrasonic exfoliation became a commonly strategy for preparing g-C_3N_4 nanosheets in water and other reagents, such as propanol, ethanol, *N*,*N*-dimethylformamide [101–106]. Zhao *et al.* [107] synthesized ultra-thin g-C_3N_4 nanosheets possessing 1 nm thick through ultrasonic exfoliation combined with thermal oxidation of bulk g-C_3N_4 with comparatively high yield (∼24%). The resultant nanosheets showed significantly improved photo-catalytic ability for hydrogen evolution.

2.3. Chemical exfoliation

Since the exfoliation efficiency of both thermal oxidation exfoliation and ultrasonic exfoliation is unsatisfactory, the chemical exfoliation method with high product field has been applied to synthesize ultra-thin g-C_3N_4 nanosheets [81,108-113]. The bulk g-C_3N_4 could be exfoliated *via* redox reactions and intercalation process *via* chemical exfoliation, ions such as H^+, Li^+, and Br^- could be effectively intercalated between the layers of bulk materials at the

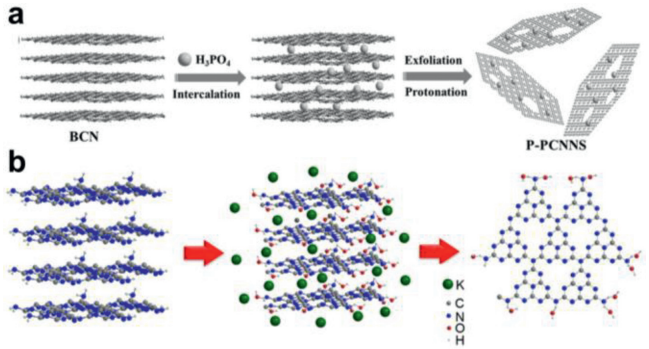

Fig. 2. Schematic illustrations of chemical exfoliation strategy for preparing g-C_3N_4 nanosheets by (a) H_3PO_4 (Reproduced with permission [115]. Copyright 2016, Wiley) and (b) KOH (Reproduced with permission [116]. Copyright 2017, Elsevier).

liquid environment under the assistance of strand nitrogens as acceptor sites, swelling the crystal, increasing the interlamellar distance, decreasing the sheets attraction, as well as bringing down the barrier potential of desquamation in a consequence, leading to the high-yield g-C_3N_4 nanosheets with a micrometers wide but few-layer thick [76]. The product yield and the thickness can be influenced by ionic species, amount of oxidant and exfoliation time. Xu and other researchers [114] firstly synthesized the unilamellar g-C_3N_4 nanosheets with the high product field up to 60% by chemical exfoliation method *via* the addition of H_2SO_4, the average thickness of as-synthesized nanosheets is approximately 0.4 nm thick, that is similar to theoretical value for unilamellar nanosheets (0.325 nm). The photo-catalytic performance of g-C_3N_4 nanosheets remarkably improved on account of increasing surface area and charge mobility. Porous g-C_3N_4 nanosheets with 1 nm thick have been prepared by Shi *et al.* [115] using phosphoric acid. Besides the intercalation effect of H^+ (Fig. 2a), the interaction between OH^- and terminal or bridged $-NH_{(2)}$ group of the triazine units in bulk material would also decrease the interlayer force and accelerate the thinning process (Fig. 2b). Mono-layered g-C_3N_4 has been obtained using KOH with a large transverse dimension with micron-grade but only 0.4 nm thick by Li and co-workers [116].

In summary, thermal oxidation exfoliation is a simple and effective approach to get a thinner nanosheet, but it should be pointed out that hazardous gas will release and abundant interface defects are generated due to the destroy of hydrogen bridge of conjugated rings as well as the polymeric chain *via* oxidation process at high temperature, besides, the break of tri-*s*-triazines cells framework could also lead to an extremely low product yield. The ultrasonic exfoliation strategy has many advantages comparing with thermal oxidation method, including a relatively high product yield, environment friendly, and the reservation of crystal texture as well as stoichiometric proportion of original g-C_3N_4. However, that is still limited by time-consuming and the destroying of the lateral size towards g-C_3N_4 *via* long-time ultrasonication, which will lead to low aspect ratio and decreased photocatalytic activities of resultant g-C_3N_4 nanosheets. Chemical exfoliation strategy can simultaneously reserve the chemical stoichiometric ratio and lateral size of the original bulk g-C_3N_4 in comparison with thermal exfoliation and ultrasonic exfoliation, besides, it also possesses other considerable superiorities, such as functionalization on the nanosheet surface, high exfoliation efficiency, as well as the probability of exfoliation into monolayer structure [72]. However, some functional groups such as amino and carboxyl will partially remain in g-C_3N_4 through chemical delamination processing, resulting in an extra amphoteric behavior of the nanosheets.

3. Modification of g-C_3N_4 nanosheets

Pristine g-C_3N_4 still suffer from unsatisfactory photo-catalytic efficiency due to the poor visible-irradiation absorption range, ready annihilation of photo-induced charges, and relatively low surface area. Many attempts have been made to deal with those problems, including construction of hetero-junctions, elements doping, defects controlling, and building nanostructures.

3.1. Hetero-junction construction

Constructing hetero-junction *via* g-C_3N_4 and other semiconductors could be regarded as a splendid method for dealing with the above problems, the annihilation of photo-induced electron-hole charges could be partly avoided in the resultant by the strong interaction in the interfaces of hetero-junctions, so far, many species of g-C_3N_4 based hetero-structures have been deeply researched [108,117-125].

3.1.1. g-C_3N_4/inorganic semiconductor hetero-structure

Zhang and other researchers [126] constructed a BiOCl/g-C_3N_4 hybrid *via* the two-step calcination-hydrothermal method and applied it as a photo-catalyst towards the decomposition of Rhodamine B as well as hydrogen generation. Their experimental results revealed that the photo-catalytic performance of as-prepared composite was improved by the successfully formation of hetero-junctions. Wang and co-workers [127] constructed a ultra-thin g-C_3N_4/Bi_2WO_6 nuclear-hull structure, which showed the best photocatalytic degradation activity towards phenol as closely 5.7-fold high as which of original g-C_3N_4, in addition, 1.9-fold compare to Bi_2WO_6 nanosheet *via* visible light irradiation, at the meantime, phenol degradation performance under full spectrum by using g-C_3N_4/Bi_2WO_6 photo-catalyst possessed 3.3 times than which of pure g-C_3N_4, in addition, 1.5-fold towards Bi_2WO_6 nanostructure by reason of the enlarged irradiation absorption range as well as separation for photo-induced charges *via* forming hetero-structure. $CoWO_4$/g-C_3N_4 hetero-structures were attained by Wang *et al.* [128], the improved photo-catalytic activity for H_2 generation could be attributed to fast photoinduced charge separation rate and transport ability benefiting from the band offset structure (Fig. 3a). Apart from TiO_2 and Bi_2WO_6, other inorganic semiconductor materials including ZnO [129], NiS [130], CdS [131], Cu_2O [132] and $Mn_{0.2}Cd_{0.8}S$ [133] also have been reported for the improved photo-catalytic behaviors of pure g-C_3N_4 nanosheets.

3.1.2. g-C_3N_4/organic macromolecular material hetero-structure

Some organic macromolecular material such as porphyrin and metal organic frameworks also can be used to form heterostructures with g-C_3N_4 nanosheets. Because of some advantages of high specific area and tunable pore size, the macromolecular materials can exhibit excellent solar harvesting performance, besides, the conjugated π bond could lead to a stable combination between organic materials and g-C_3N_4 through the generation of π-π bond, which accordingly resulted in stable structure and outstanding photo-catalytic activity. UiO-66 coupled with g-C_3N_4 nanosheets has been constructed by Mardiroosi *et al.* [134], the enhanced photo-catalytic degradation capacity putted down to formation of hetero-junction *via* UiO-66 and g-C_3N_4, nevertheless, electrons could effectively transfer to g-C_3N_4 under the force of built-in potential produced through hetero-junction structure, giving rise to a enhanced response towards light range and the decreasing of annihilation for electron/hole pairs (Fig. 3b). Xu *et al.* [135] utilized another metal-organic framework BIF-20 to constructed heterostructure with g-C_3N_4 nanosheets, leading to a significantly enhanced CO_2 photo-reduction rate. Other organic macromolecular

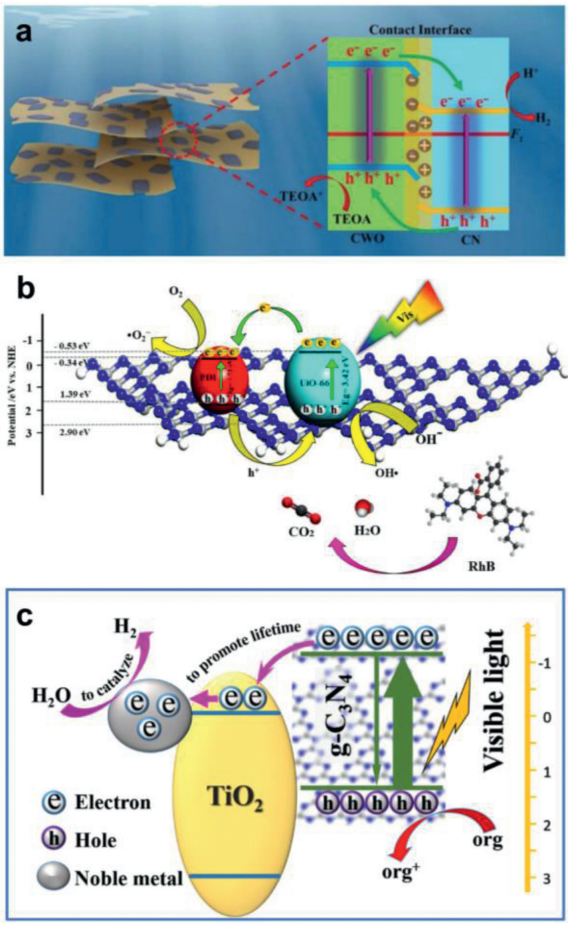

Fig. 3. (a) Schematic illustration for photocatalytic mechanism of $CoWO_4$/g-C_3N_4 photocatalysts. Reproduced with permission [128]. Copyright 2017, Springer. (b) The suggested photocatalytic RhB degradation mechanism over 30PCN@UiO-66 system under visible-light illumination. Reproduced with permission [134]. Copyright 2021, Elsevier. (c) Mechanism of the photo-generated charge transfer and induced photo-catalytic processes for H_2 evolution in the presence of methanol under visible-light irradiation on g-C_3N_4/metal hetero-structure. Reproduced with permission [144]. Copyright 2018, Elsevier.

materials including tetraphenylporphyrin [136], ZIF-8 [64], and Ni-MOF [137] also been widely studied for the elevation of photo-catalytic activity towards g-C_3N_4 nanosheets.

3.1.3. g-C_3N_4/metal hetero-structure

Recently, forming a hetero-junction between metal nano-particles and g-C_3N_4 nanosheets has been studied as an effective method to improve the photo-catalytic performance of g-C_3N_4 [101,138-141]. On account of the surface plasmon resonance effect, the metal nano-particles could be the high-efficiency electron acceptors [142], thus accelerating the separation rate of photo-generated charges in g-C_3N_4 nanosheets, in the meantime, increasing the light absorption. Wang [143] synthesized a g-C_3N_4/Pt(111) hero-structure with improved photo-reaction activity of CO oxidation. Zhang and co-workers [144] enhanced the photo-catalytic hydrogen evolution ability of g-C_3N_4 nanosheets facing visible-light irradiation *via* decorating Ag, Au and Pt, compared with original g-C_3N_4, the hydrogen evolution ability of the optimal resultant could exhibit about a 14-fold increase, because of the effective separation of the photo-induced charge pairs as well as the co-catalytic action of noble metal nanoparticles (Fig. 3c).

3.1.4. g-C_3N_4/carbon material hetero-structure

Carbon quantum dots, reduced graphene oxide and multiwall carbon nanotube brought many notices because of the extraordinary chemical as well as physical characters [145–148], in recent years, it have been deeply studied and subsequently proved that decorating g-C_3N_4 nanosheets with carbon quantum dots would accelerate the migration for photo-induced charges effectively by π-π bond force generated *via* CQDs and g-C_3N_4 nanosheets, which could inhibit photo-induced carries annihilation partly *via* the formation of intermolecular forces [149]. A C_3N_4/rGO/C_3N_5 sandwich heterojunction was synthesized *via* a post-annealing process by Liu *et al.* [150], the as-prepared hybrid photo-catalyst exhibited much superior H_2 evolution activity compared with pure g-C_3N_4 nanosheets because of high interfacial carries separation migration ability.

What is more, the materials mentioned above also been synergistically utilized to form ternary or quaternary structure for enhancing the photo-catalytic behavior of g-C_3N_4 nanosheets [119,151-154]. Deng *et al.* [95] constructed ternary Ag/N-GQDs/g-C_3N_4 hybrids, such as-synthesized ternary structure exhibited 92.8% as well as 31.3% degradation of tetracycline through simulated sunlight and near-infrared illumination, respectively, providing a novel strategy towards effective photo-catalytic reaction under full-spectrum illumination. Shi *et al.* [155] synthesized the ternary Ag_3PO_4/$Co_3(PO_4)_2$/g-C_3N_4 hetero-junction with enhanced photo-catalytic degradation efficiency, the as-prepared hybrid photo-catalyst could reach a superb removal of tetracycline (88%) after 120 min facing visible irradiation.

With such construction of hetero-junctions, the specific area enlarged, at the same time, the band position changed, leading to a higher solar harvesting efficiency and separation rate of photo-induced charges, which can effectively elevate the photo-catalytic behavior of g-C_3N_4 nanosheets.

3.2. Homo-junction construction

Apart from forming hetero-structure, using g-C_3N_4 itself for constructing the g-C_3N_4/g-C_3N_4 homo-junction also attracted attentions in recent years. A novel g-C_3N_4 nanosheets recombined with C_3N_4 QDs nanocomposites was synthesized by Xu *et al.* [156], the resultant exhibited more stable and excellent behavior in comparison with unitary g-C_3N_4 nanosheets towards the detection of PDGF-BB. Qiao with co-workers [157] obtained the g-C_3N_4/g-C_3N_4 Z-scheme homo-junction with improved rhodamine degradation rate, which was about 15.4-fold compared with which of bulk g-C_3N_4. The increasing photo-catalytic capacity could put down to huge exposed specific area, efficient separation and excellent redox abilities of the photo-induced charges with a formation for the homo-junction.

3.3. Doping

Another method to improve photo-catalytic behavior of g-C_3N_4 nanosheets is doping, typically, metal with nonmetal element doping for g-C_3N_4 have been studied for the reason of partly adjusting crystallographic, electronic as well as band positions to enhance photo-catalytic capacity *via* broadening irradiation response range, improving photo-generated charges migration, and lengthening life-span of photo-induced carriers. Doping with nonmetal species including B, N, Cl and so on has been widely reported [158–161]. Jiang and other researchers [47] fabricated N doped g-C_3N_4 nanosheets with a midgap state created by N doping, as a consequence, the as-synthesized g-C_3N_4 nanosheets showed higher photo-catalytic capacity towards tetracycline degradation than original g-C_3N_4 due to the easy generation and transport of electrons *via* the midgap state. A K, P, O, S-doped C_3N_4 has been constructed *via* Deng *et al.* [162], such co-doping of above elements towards g-C_3N_4 broadened the light absorption, besides quickened the migration for photoinduced carries, leading to the superior

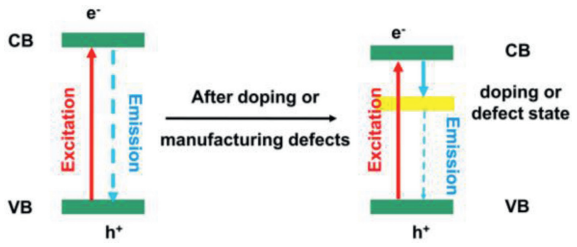

Fig. 4. The charge transfer mechanism towards doping and defect control.

photo-catalytic behavior for antibiotics destroying in natural water facing visible light irradiation. Yang *et al.* [163] constructed O-doped g-C_3N_4 composites, leading to the elevated CB edge as well as the detachment and movement rate of photoinduced charges, the as-prepared samples showed highly improved photo-catalytic hydrogen evolution ability, which was approximated 5.2-fold compared with which of original g-C_3N_4 facing ultraviolet-visible light. The nanostructure for g-C_3N_4 catalyst doped with metal elements like Ni, Co, Na, K, Sr and Fe [164–166] also been widely studied for achieving superior photo-catalytic performance of g-C_3N_4. An Al-doped g-C_3N_4 hybrid photo-catalyst was constructed by Choi and co-workers [167]. The introduction of Al atom doping sites could effectively modify the band structure of pure g-C_3N_4 with a midgap state, leading to the increased photo generated charges of the as-prepared photo-catalyst.

3.4. Defect control

Since some researchers have proved that defects are efficient captures for electrons [168,169], defect controlling could be an effective way for dealing with the ready recombination of photo-induced charges of g-C_3N_4 nanosheets. Dong and co-workers [170] demonstrated that photo-excited charges would separate more efficiently in carbon vacancy-modified g-C_3N_4 (Ns-g-C_3N_4) than in pure one due to the capture ability of vacancy, at the same time, the carbon vacancy-induced defect states in the band gap extended the response spectrum for g-C_3N_4 to the whole visible area, leading to the efficient photo-reduction towards NO under visible light. Li and co-workers [171] studied a high-temperature polymerization strategy to obtain N vacancy-modified g-C_3N_4 with improved photo-catalytic hydrogen evolution activity, the band structures were modified due to the variation of C/N ratio, favoring the separation speed of photo-excited charges with the light response range.

With doping or defect control, a midgap could be introduced into bandgap of g-C_3N_4 nanosheet, which would be an effective electron capture center, leading to the decreased recombination rate of photo-induced charges. Besides, the bandgap of g-C_3N_4 nanosheet would narrow after manufacturing defects, consequently, the light absorption range would broaden, resulting in the better photo-catalytic performance (Fig. 4).

3.5. Structure design

Moreover, structure design of g-C_3N_4 nanosheet has been researched for improving those photo-catalytic performance *via* enlarged surface area and shortened migration distance of photo-induced charge carriers. Constructing of porous structure and ultra-thin structure were two mainly strategies in this area [34,172-174]. Li *et al.* [175] prepared holey g-C_3N_4 nanosheet (hCNNS) photo-catalysts with a ultra-thin thickness and high pore volume *via* a two-step calcination, leading to a large surface area, the as-synthesized hCNNS possessed more surface reactive sites, strengthened photoredox ability, shortened the migration distance of photo-induced charges, and widened the irradiation response range, as a consequence, the visible-light-driven photocatalytic hydrogen generation speed was significantly elevated in contrast with original g-C_3N_4. Liu and co-workers [176] constructed mesoporous g-C_3N_4 nanosheets *via* hydrothermal treatment, it was found that the mesoporous nanostructure achieved a significantly enhanced hydrogen producing speed of 136.9 μmol/h, which was 15 times higher than pristine g-C_3N_4. Ultrathin g-C_3N_4 nanosheets were attained *via* rapid high-temperature treatment by Zhang *et al.* [96], numerous active sites for photocatalytic repercussion with enhanced solar harvesting performance were obtained through the remarkable enlarged specific region, besides, stronger driving force was acquired through the enlarged bandgap structure because of quantum confinement effect in thinner g-C_3N_4 nanosheets, realizing a 25.5-folds improved visible-light photocatalytic H_2-producing behavior compared with pure g-C_3N_4.

As a summary, since pristine g-C_3N_4 has the disadvantages such as poor irradiation absorption range, ready annihilation of photo-induced charges, and relatively low surface area, many modification approaches have been studied. The construction of hetero-structure and homo-structure effectively promoted charges separation *via* the matched energy level, doping and defect control of g-C_3N_4 nanosheet could narrow the pristine bandgap as well as introduce a midgap, extending the light utilization range as a consequence, the structure design could increase specific surface area of g-C_3N_4 nanosheet to provide more active sites for the photocatalytic reaction. However, there are still some questions such as the more suitable band match for hetero-junctions, the optimum concentration of doping as well as defects, and the less damage of original triazine ring during structure design, which should be further studied in the future.

4. Mechanism of g-C_3N_4-based hetero-structures

Among the strategies which were introduced above for the improvement towards the photo-catalytic performance of g-C_3N_4 nanosheet, a construction for hetero-structure could be the most general one due to many merits, including effective separation of photo-induced charge carries, high harvesting of solar light, and the relative low cost. As a consequence, the photo-generated charge transfer mechanism of hetero-junctions has been widely studied over the years.

4.1. Type-II hetero-structure

The traditional type-II hetero-junction is formed by g-C_3N_4 and other semiconductors. The difference of band positions between the multiple semiconductors leading to the generation of band bending in the hetero-junction. When exposed to light, the photo-generated electrons would migrate from the higher CB level to the lower one because of the formation of built-in electric field generated from the band bending, while the photo-induced holes migrate in the opposite direction. Specially, the wavelength of light irradiation at which the photo-reaction could occur corresponds to a narrower band gap of those semiconductors. Therefore, the formation of type II hetero-junction would extend the light response range and improve the photo-excited charge separation, which could in turn enhance the photo-catalytic performance [177].

Yi and co-workers [178] synthesized Nb_2O_5/g-C_3N_4 nanosheets hybrid, the g-C_3N_4 nanosheets have more negative CB band positions than those of Nb_2O_5, as a consequence, the photo-induced electrons could migrate from g-C_3N_4 to Nb_2O_5 (Fig. 5a). Since the CB level of Nb_2O_5 is higher than the H^+/H_2 potential, the photo-generated electrons in Nb_2O_5 could split water to produce H_2 directly. Similarly, Majumdar *et al.* [179] constructed Bi_4NbO_8Cl/g-

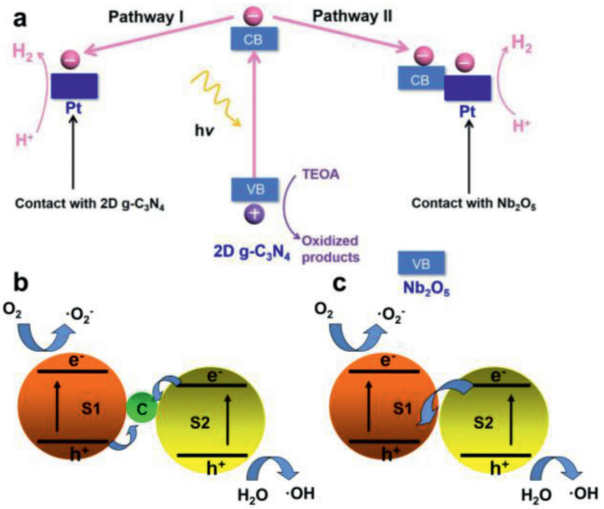

Fig. 5. (a) Schematic of electron transfer in Nb_2O_5/g-C_3N_4 nanosheets hybrid photo-catalyst. Reproduced with permission [178]. Copyright 2021, Elsevier. The charge transfer mechanism of SCS (b) and SS (c) Z-scheme.

C_3N_4 hetero-structure, according to calculation results, the CB and VB band positions of Bi_4NbO_8Cl are about −0.54 and 2.07 eV, while those of g-C_3N_4 are about −1.20 and 1.84 eV, respectively, because of the formation of type-II hetero-junction, the photo-excited electrons in the CB of g-C_3N_4 could inject into that of Bi_4NbO_8Cl, while opposite transfer occurring in the photo-induced holes in the VB of Bi_4NbO_8Cl, the effective separation of photo-induced charges could improve the activity of photo-catalytic degradation of oxytetracycline significantly as a consequence. Other type-II hetero-junction hybrid photo-catalysts such as NiS/g-C_3N_4 [130], Bi_2WO_6/g-C_3N_4 [180], BiOCl/g-C_3N_4 [104] and g-C_3N_4 nanosheet/$ZnIn_2S_4$ nanoleaf [48] have also been reported as efficient photo-catalysts for pollution degradation, water splitting and organic synthesis on account of the effective separation of photo-excited carriers and enlarged light response range.

4.2. Z-scheme hetero-structure

The type-II hetero-junctions provided effective charge separation, however, the lower CB level and the higher VB level of which limited the redox ability of as-prepared photo-catalysts, leading to a weakened performance for photo-catalytic reaction. In such case, a new type of charge transfer mechanism has been studied, which was called Z-scheme hetero-structure, simultaneously achieve effective separation of photo-excited charges as well as strong redox ability. The Z-scheme hetero-structure could mainly be divided into two types: Ionic-state and all-solid-state, the latter can be further divided into semiconductor-conductor-semiconductor (SCS) Z-scheme hetero-junctions and semiconductor-semiconductor (SS) Z-scheme hetero-junctions.

In the SCS Z-scheme hetero-junctions, appropriate conductors such as noble metal particles, graphene and many other conductive materials can be inserted between semiconductors to provide the pathway for electron migration to improve the efficiency of charge transport and separation [181,182]. The electrons generated in the CB of one semiconductor, migrated to noble metal particles which has high work function, and subsequently recombined with holes induced in the other semiconductor (Fig. 5b), simultaneously, the remaining photo-generated electrons in higher CB and holes in lower VB of two semiconductors could be applied to the photo-catalytic reduction and oxidation reactions, respectively.

Wu and co-workers [183] employed many approaches to study Z-scheme mechanism towards $BaTiO_3$/Au/g-C_3N_4 hybrid composites. The radical scavengers experiment indicated O_2^- radicals as an active species in photo-catalytic degradation, VB XPS and Mott-Schottky plots experiments calculated the band positions of both $BaTiO_3$ and g-C_3N_4, considering that the CB level of $BaTiO_3$ was less-negative comparing with H^+/H_2 potential, photo-induced electrons prefer to accumulate in g-C_3N_4 rather than $BaTiO_3$, as a consequence, the photo-excited charges transfer pathway followed Z-scheme, the H_2 evolution and photo-degradation performance of Rhodamine B improved due to high separation rate of the photo-excited charges. Other SCS Z-scheme system such as Ag/$AgVO_3$/carbon-rich g-C_3N_4 [184], $W_{18}O_{19}$/Au/g-C_3N_4 [185] and ZnO/Au/g-C_3N_4 [186] have also been widely constructed for the improving photo-catalytic performance in water splitting, pollution mitigation, and CO_2 reduction of g-C_3N_4 nanosheets.

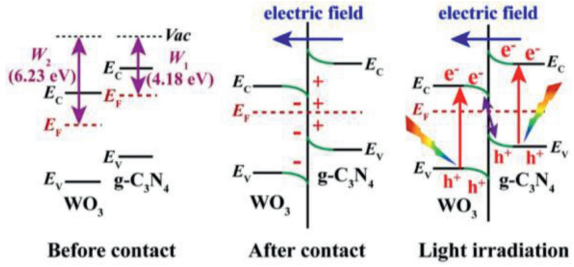

Fig. 6. The S-scheme charge transfer mechanism between WO_3 and g-C_3N_4 under light irradiation. Reproduced with permission [61]. Copyright 2019, Elsevier.

However, high-cost and shielding effect limited the widely adhibition of noble metals such conductor-assistant Z-scheme hetero-structure [63], different from SCS Z-scheme system, the photo-excited charges could directly transfer between two semiconductors in the SS Z-scheme photo-catalyst. In this manner, the photo-catalytic efficiency can be further increased because of the shortened migration distance of the photo-excited charges (Fig. 5c) [187–194]. A TiO_2/g-C_3N_4 composite which followed Z-scheme mechanism was fabricated by Liu *et al.* [195]. Mott-Schottky plots were tested to calculate the band positions of both TiO_2 and g-C_3N_4, electron spin resonance experiment indicated O_2^- radicals as an active species, on account of the less-negative CB level towards TiO_2 compared of O_2^-/O_2 potential, the as-prepared composite showed decreased photo-excited charges recombination rate and prolonged lifetime *via* the formation of Z-scheme hetero-junction, leading to the enhanced photo-catalytic degradation performance. Zhang and co-workers [196] employed many approaches to study Z-scheme mechanism towards V_2O_5/P-g-C_3N_4 hybrid composites. Both trapping agent and electron spin resonance testing indicated h^+ and O_2^- radicals as an active species in photo-catalytic degradation, considering that the CB level of V_2O_5 was less-negative comparing with O_2^-/O_2 potential, the O_2^- radicals were generated by the photo-excited electrons in g-C_3N_4 rather than V_2O_5, the photo-degradation performance of methyl orange improved due to high separation rate of the photo-excited charges.

4.3. S-scheme hetero-structure

Another hetero-structure which is called step-scheme (S-scheme) hetero-structure has also been discussed by Fu *et al. via* the ultra-thin WO_3/g-C_3N_4 hetero-junction photo-catalysts [61] to remedy the drawbacks of type-II hetero-junction as well as further improve photo-catalytic performance. Under irradiation, the photo-induced electrons in WO_3 and the holes in g-C_3N_4 were recombined under the effect of internal electric field between two semiconductors (Fig. 6), remaining holes in WO_3 and electrons in g-C_3N_4 to achieve photo-catalytic oxidation and reduction reactions, respectively. This S-scheme charge carrier transfer mechanism en-

sures the as-constructed WO_3/g-C_3N_4 hybrid composites with enhanced electron–hole pair separation ability and elevated redox capacity, leading to the fast photo-catalytic water splitting rate. As a result, the H_2 evolution rate of as-prepared composite was improved, which was 1.7-fold compared with pristine g-C_3N_4.

5. Applications of g-C_3N_4-based photo-catalysts

The g-C_3N_4-based photo-catalysts possess a large surface area, which can contribute high light harvesting and numerous active sites to accelerate the photo-catalytic reaction, and an appropriate band structure for light absorption and photo-catalytic redox reaction, besides, the good accessibility and high stability against temperature, acid or alkali solutions also make the g-C_3N_4 nanosheets-based photo-catalysts become the extensive applications such as pollution degradation, energy generation, nitrogen fixation. Herein, some remarkable applications will be listed as follows.

5.1. Photo-degradation of environmental pollutants

Semiconductor photo-catalysis is an excellent material to solve the environment questions. On account of the appropriate band structure and good stability, the g-C_3N_4 nanosheets has widespread application towards the photo-catalytic reaction of numerous water pollutants, such as organic dye-stuffs [108,129,134,197-201], aromatic compounds [202,203], antibiotic [47,95,120,204], heavy metal [60]. The removal of air contaminants such as NO [34,170,173] and CO [143] has also been investigated.

5.1.1. Water pollutants

Amorphous Cu-doped FeOOH nanoclusters/ultra-thin g-C_3N_4 nanosheets hybrid photo-catalyst was synthesized by Zhang *et al.* [94], when exposed to visible light, the resultant could decolorize ~98.7% MB within 40 min, the highly enhanced photo-catalytic ability (more than 8.1 times) in comparison with original g-C_3N_4 nanosheets endowed the resultant photo-catalyst with prospective industrialization applicability. He *et al.* [149] obtained graphene–carbon quantum dots/g-C_3N_4 nanosheets composite *via* the hydrothermal way, the MO removal ratio of the as-prepared photo-catalyst was up to 91.1% under 4 h-visible light irradiation, which achieved approximately 7.6-fold improvement of original g-C_3N_4 (Figs. 7a and b). Dong and co-workers [168] utilized hydrochloric acid to gain ultra-thin g-C_3N_4 nanosheet for elevated photo-catalytic degradation rate of RhB. As a result, the RhB could be decomposed completely after 75 min-exposure of the visible light. Yang *et al.* [200] constructed Nb_2O_5/g-C_3N_4 photo-catalyst *via* the one-step heating approach, realizing a better photo-catalytic performance, 95% of RhB, 15% of MO and 87% of MB were degraded after one hour facing visible irradiation by as-prepared materials, respectively. Zhang and co-workers [204] prepared $NaNbO_3$/g-C_3N_4 composites to deal with the ofloxacin degradation, the as-prepared samples exhibited increased photo-catalytic ability under simulated sunlight, 99.5% of ofloxacin was removed within 30 min by the optimum sample. The effective removal of highly toxic Cr^{5+} to Cr^{3+} using visible irradiation as driving force was successfully achieved *via* g-C_3N_4 nanosheets-based photo-catalysts such as g-C_3N_4/C/Fe_2O_3 [205] and ternary Au/g-C_3N_4/$W_{18}O_{49}$ hybrid composite [60], which could reduce more than 80% of Cr(VI) within 30 min (Figs. 7c and d). The photo-degradation of aromatic compounds such as phenol has been studied by Wang *et al.* [127], the results illustrated the constructed g-C_3N_4/Bi_2WO_6 core-shell structure possessed superior photo-catalytic phenol degradation activity towards simulated sunlight as well as visible light due to the strong oxide ability and decreased recombination of photo-generated charges.

5.1.2. Gas pollutants

Wang *et al.* [143] prepared the g-C_3N_4/Pt (111) nanostructure for the effective photo-catalytic oxidation of CO. Huang *et al.* [173] fabricated porous g-C_3N_4 nanosheets, on account of the merits such as huge surface area as well as excellent charge carriers separation ability, ultra-thin g-C_3N_4 has efficient application in visible-light-driven photo-catalytic NO mitigation, achieving a 5.5-fold increasing in comparison with original g-C_3N_4. Dong [166] prepared Sr-modified g-C_3N_4 nanosheets for the elevated photo-catalytic NO reduction capacity. A redshift of absorption

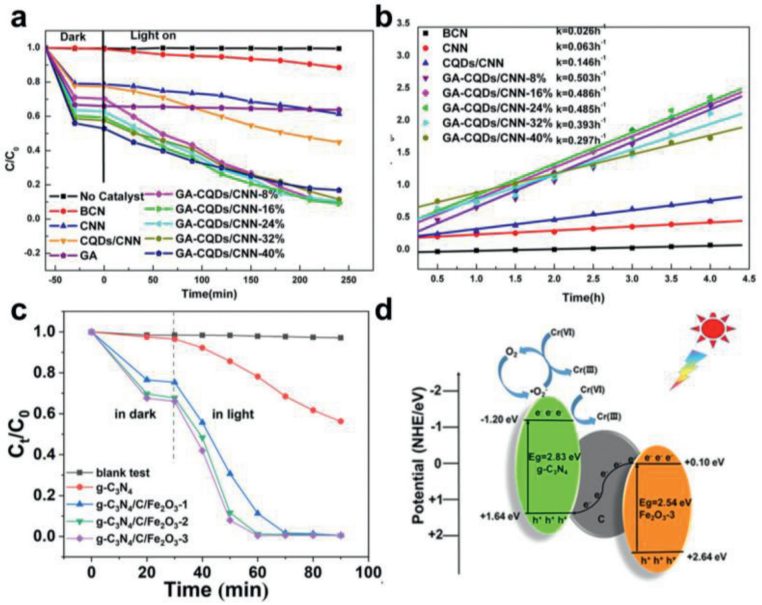

Fig. 7. (a) Absorptive, photo-catalytic removal of aqueous MO over graphene-carbon quantum dots/g-C_3N_4 nanosheets composite under visible light ($\lambda > 420$ nm), and (b) corresponding kinetic simulation curves. (a, b) Reproduced with permission [149]. Copyright 2018, Elsevier. (c) Cr(VI) reduction efficiency by different photocatalysts and (d) schematic illustration of the reduction of Cr(VI) by g-C_3N_4/C/Fe_2O_3 under light irradiation. (c, d) Reproduced with permission [205]. Copyright 2021, American Chemical Society.

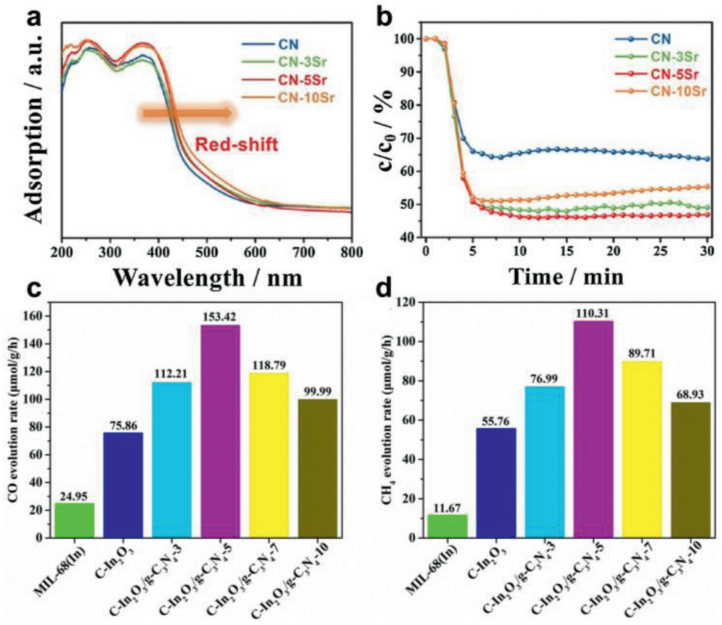

Fig. 8. The UV–vis spectra (a) and photocatalytic activity for NO removal (b) of as-prepared samples. (a, b) Reproduced with permission [166]. Copyright 2018, Elsevier. (c) Production rate of CO and (d) Production rate of CH_4 for C-In_2O_3/g-C_3N_4 composite under ultraviolet light. (c, d) Reproduced with permission [206]. Copyright 2021, Elsevier.

edge occurred after doping, resulting in the extended light adsorption (Fig. 8a), at the meantime, the intercalation of Sr enlarged the bond length of g-C_3N_4, resulting in the weakened Coulomb interaction for gas molecules with easy activation of O_2 molecules on the catalyst surface. The composites have increased NO removal rate compared with original g-C_3N_4 nanosheets (Fig. 8b). Moreover, Jiang and co-workers [39] also studied the photo-oxidation behavior of NO to nitrate *via* N-doped TiO_2/g-C_3N_4 hetero-structure, the removal ratio of resultant photo-catalyst towards ppb-level NO could reach 46.1% within 30 min under visible light illumination.

5.2. Energy generation

5.2.1. CO_2 reduction

The hydrocarbon fuel has many merits including renewable and clean, according to the ability for the coverting of CO_2 into CH_4, the applications of CO_2 reduction of photo-catalysts have been widely studied.

A C-In_2O_3/g-C_3N_4 composite was fabricated by Xu *et al.* [206] *via* the solvent method for the photo-reduction towards CO_2, the CO and CH_4 evolution rate of 153.42 μmol g^{-1} h^{-1} and 110.31 μmol g^{-1} h^{-1} were achieved under ultraviolet light irradiation, Especially, the large surface area towards irradiation as well as decreased recombination of photo-excited charges endowed the resultant with significantly enhanced photo-catalytic performance (Figs. 8c and d). Liu and co-workers [136] obtained cobalt meso–tetra-phenylporphyrin/g-C_3N_4 hetero-structure, the high specific surface area and porous structure with suitable hole size favored CO_2 adsorption, at the meantime, the promoted separation ability of photo-induced electrons and holes increased electron utilization efficiency, leading to the superior CO_2 catalytic conversion performance. Nie *et al.* [194] fabricated the g-C_3N_4/ZnO composite with a 4.1 times CH_3OH production rate compared to pristine g-C_3N_4. The PL measurement was carried out to certify the existence of ·OH in photo-catalytic reaction. Xia and co-researchers [52] constructed g-C_3N_4 nanosheets with a thickness ~3 nm *via* thermal exfoliation approach under the NH_3 atmosphere, the obtained nanosheets exhibited remarkably enhanced photo-catalytic CO_2 reduction performance. Other g-C_3N_4 nanosheets-based photo-catalysts such as BIF-20@g-C_3N_4 [135], g-C_3N_4/WO_3 [207], and g-C_3N_4/CdS [208] also be constructed for the effective CO_2 photo-catalytic reduction.

5.2.2. Water splitting

Apart from hydrocarbon fuel, hydrogen energy has also been regarded as a potential and promising fuel for the substitution of traditional fossil energy due to the renewability and high energy storage [209]. Photo-catalytic decomposition of water by photo-catalysts could be a effective method for generating hydrogen. Numerous photo-catalysts have been studied to achieve the photo-catalytic hydrogen generation, nonetheless, low solar energy utilization ratio and poor redox capacity due to improper band structure limited the practical applications of those photo-catalysts. Considering the g-C_3N_4 nanosheets-based materials with suitable band position and large surface, the hydrogen evolution of which has been discussed as a consequence [158,163,210,211].

He *et al.* [130] constructed the g-C_3N_4/NiS hybrid hetero-structure with an excellent photo-catalytic H_2 evolution ability of 29.68 μmol/h under visible light illumination, which could be comparable to some samples using Pt as cocatalyst. The CdS/g-C_3N_4 nanocomposite was prepared [131] for the effective photo-catalytic H_2 production performance (2120 μmol g^{-1} h^{-1}) due to the enhanced charges separation and transfer rate by the formation of hetero-junction (Fig. 9). In addition to high H_2 generation rate, the recyclability and durability also made as-prepared photo-catalysts eligible for widespread practical application. A ternary CdS/RGO/g-C_3N_4 composite was constructed by Jo *et al.* [182], the resultant showed enhanced photo-catalytic hydrogen generation performance compared with CdS/g-C_3N_4 photo-catalysts, proving the RGO as an efficient electron mediator. PL emission spectra and transient photo-current measurements were applied to further demonstrate the charge separation and migration, the as-prepared composite showed decreased photo-excited charges recombination rate and prolonged lifetime *via* the formation of Z-scheme hetero-junction, leading to the increased photo-catalytic hydrogen generation ability. Tahir *et al.* [212] fabricated g-C_3N_4/$TiH_{1.92}$ photo-catalyst with a highly effective H_2 evolution ability of 75.55 μmol/h in visible light region. What is more, Zhang *et al.* [144] utilized no-

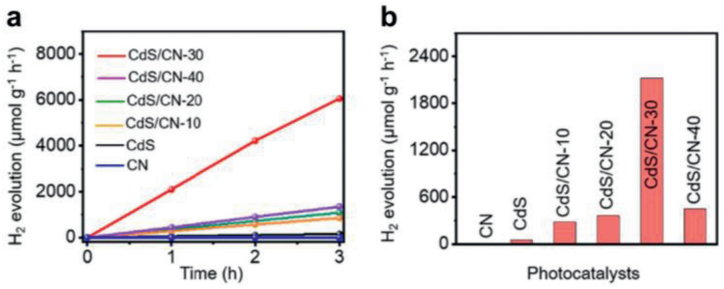

Fig. 9. Photocatalytic activity in H_2 production. (a) The time-dependent H_2 production curves of different photocatalysts. (b) H_2 generation rate of different photocatalysts; All the photocatalytic H_2 generation tests were measured under visible-light irradiation ($\lambda > 400$ nm) and in 80 mL aqueous solution containing 10 vol% sacrificial reagents without cocatalysts. Reproduced with permission [131]. Copyright 2022, Elsevier.

ble metals (Ag, Au and Pt) to decorate g-C_3N_4/TiO_2 nanocomposite for the further improving of photo-catalytic H_2-production activity to 519.73 μmol g^{-1} h^{-1}. Other g-C_3N_4 nanosheets-based hetero-structures such as SnS_2/g-C_3N_4 nanosheet [213], $NiCo_2O_4$/g-C_3N_4 [214], ruthenium phosphide/g-C_3N_4 [117], WS_2/g-C_3N_4 [133], g-C_3N_4/rGO/PDIP [152], $FeSe_2$/g-C_3N_4 [215] also have been reported as efficient photo-catalysts for the photo-catalytic hydrogen evolution.

Besides constructing g-C_3N_4-based hetero-structures, controlling of morphology and defects could also been widely applied in photo-catalytic H_2-production of g-C_3N_4 to achieve much better performance [171,176,216]. Zhang *et al.* [96] fabricated ultra-thin g-C_3N_4 nanosheets with abundant mesopores and macropores structure, leading to excellent increased (25.5 times) light-driven photo-catalytic H_2 generation ability. Defects rich g-C_3N_4 nanosheets was constructed [172], the resultant exhibited significantly improved photo-catalytic H_2 evolution rate of 761.8 ± 4.3 μmol g^{-1} h^{-1} under simulated sunlight illumination.

5.3. Other applications

Furthermore, g-C_3N_4 nanosheets hybrids were also applied in photo-catalytic disinfection [154], N_2 fixation [169], organic synthesis [217], and so on. Li *et al.* [218] synthesized Ag_2WO_4/g-C_3N_4 photo-catalyst with significantly enhanced photo-catalytic disinfection performance, as a result, *Escherichia coli* cells have been distorted and destroyed totally by as-prepared hybrid photo-catalyst within 90 min. Cao and co-workers [169] fabricated ultra-thin sulfur-doping g-C_3N_4 (SCNNSs) possessing carbon vacancies, due to the superior N_2 molecules adsorption and activation ability, as well as the effective photo-generated charge carries separation, the N_2 fixation rate could reach 5.99 mmol L^{-1} h^{-1} g_{cat}^{-1} after 4-h simulated sunlight illumination *via* the obtained SCNNSs.

Apart from photo-catalytic field, g-C_3N_4 nanosheets based composites also utilized to perform as lithium-ion batteries [219], photoelectrochemical devices [220], supercapacitor [221], fluorescence sensor [222,223], and bio-imaging and bio-sensor [156,224] and so on. With many advantages, such as low cost, good temperature and chemical stability, tunable electronic structure, appropriate band position, and acceptable redox potential, various application possibilities of g-C_3N_4 nanosheets-based photo-catalysts will be explored in the near future.

6. Summary and perspective

This review summarizes the exfoliation methods, modification strategies, photo-catalytic mechanism and applications of g-C_3N_4 nanosheets, numerous progresses have been achieved in the fabrication and functionalization of g-C_3N_4 nanosheets for efficient water splitting, pollution mitigation, CO_2 photo-reduction, and so on in the past three years. To conclude, the g-C_3N_4 nanosheets can be attained *via* three approaches: thermal oxidation, ultrasonic, and chemical exfoliation. In order to deal with poor light absorption range, high recombination rate of photo-induced charges, and low surface area of g-C_3N_4, many modification strategies such as construction of hetero-junctions, elements doping, defect control, and structure design have been widely studied and reported, the synthesis of those g-C_3N_4-based photo-catalysts improved the production ability and separation rate of photo-induced charges *via* the formation of type-II hetero-junctions, Z-scheme and S-scheme hetero-junctions, in addition, the redox ability can be further enhanced in the Z-scheme and S-scheme system, leading to a better photo-catalytic performance in environmental pollution degradation, energy production, nitrogen fixation, disinfection and so on.

In spite of the great achievements of g-C_3N_4 nanosheets over the years, there are still many challenges for this material in photo-catalysis. Firstly, although many exfoliation ways have been studied for attaining ultra-thin g-C_3N_4 nanosheets, the decrease of lateral size, relative low product yield, and secondary pollution still exist. We could boost pressure during the thermal exfoliation process, cutting down the reaction temperature and time, leading to the less destroy of lateral size. We could also combine those exfoliation methods to elevate the product yield. Secondly, since the reports focus more on the improvement of photo-catalytic efficiency, actual mechanisms toward photo-catalytic reaction especially the water splitting and CO_2 reduction are still up in the air yet until now, we could use the theoretical computational simulations to analyze the photo-induced charge carrier transfer pathway and dynamics to further study the mechanism. Besides, the potential applications of g-C_3N_4 nanosheets could further extend. In view of the facile synthesis, low price, non-toxicity, high stability against temperature and chemicals, and appropriate band gap and band position, the g-C_3N_4-based photo-catalysis could be widely applied in the near future.

Declaration of competing interest

The authors declare that they have no known competing financial interests or personal relationships that could have appeared to influence the work reported in this paper.

Acknowledgment

The authors gratefully acknowledge the financial support by the Natural Science Foundation of China (Nos. 21872102 and 22172080).

References

[1] A. Fujishima, K. Honda, Nature 238 (1972) 37–38.
[2] Z. Wang, C.Y. Yang, T.Q. Lin, et al., Adv. Funct. Mater. 23 (2013) 5444–5450.
[3] B. Liu, H.M. Chen, C. Liu, et al., J. Am. Chem. Soc. 135 (2013) 9995–9998.
[4] J.C. Yu, J. Yu, W. Ho, Z. Jiang, L. Zhang, Chem. Mater. 14 (2002) 3808–3816.

[5] J.G. Yu, J.X. Low, W. Xiao, P. Zhou, M. Jaroniec, J. Am. Chem. Soc. 136 (2014) 8839–8842.
[6] R. Asahi, T. Morikawa, T. Ohwaki, K. Aoki, Y. Taga, Science 293 (2001) 269–271.
[7] C. Han, Z. Chen, N. Zhang, J.C. Colmenares, Y.J. Xu, Adv. Funct. Mater. 25 (2015) 221–229.
[8] H. Shuai, J. Wang, X.G. Wang, G.X. Du, Materials 14 (2021) 6474.
[9] A. Tanaka, K. Hashimoto, H. Kominami, J. Am. Chem. Soc. 136 (2014) 586–589.
[10] X.Y. Xiong, Y.R. Jin, H.W. Wang, et al., Mater. Chem. Phys. 281 (2022) 125824.
[11] Z. Liu, D.D. Sun, P. Guo, J.O. Leckle, Nano Lett. 7 (2007) 1081–1085.
[12] I. Fatimah, G. Purwiandono, H. Hidayat, et al., Nanomaterials 11 (2021) 3012.
[13] Y.X. Guo, H.W. Huang, Y. He, et al., Nanoscale 7 (2015) 11702–11711.
[14] Z.Q. Zheng, F. Han, B. Xing, X.B. Han, B.X. Li, J. Colloid Interface Sci. 624 (2022) 460–470.
[15] S. Kohtani, M. Koshiko, A. Kudo, et al., Appl. Catal. B: Environ. 46 (2003) 573–586.
[16] D. Philo, S.Q. Luo, C. He, et al., Adv. Funct. Mater. 32 (2022) 2206811.
[17] Z.G. Yi, J.H. Ye, N. Kikugawa, et al., Nat. Mater. 9 (2010) 559–564.
[18] Z.G. Zou, J.H. Ye, K. Sayama, H. Arakawa, Nature 414 (2001) 625–627.
[19] D.M. Schultz, T.P. Yoon, Science 343 (2014) 1239176.
[20] N. Torkian, A. Bahrami, A. Hosseini-Abari, et al., Environ. Res. 207 (2022) 112157.
[21] T. Cheng, Q. Ma, H. Gao, et al., Mater. Today Chem. 23 (2022) 100750.
[22] Y.Q. Yang, L.C. Yin, Y. Gong, et al., Adv. Mater. 30 (2018) 1704479.
[23] G. Yang, P. Qiu, J.Y. Xiong, X.T. Zhu, G. Cheng, Chin. Chem. Lett. 33 (2022) 3709–3712.
[24] L.Z. Liu, T.P. Hu, K. Dai, J.F. Zhang, C.H. Liang, Chin. J. Catal. 42 (2021) 46–55.
[25] H. Yang, Z.L. Jin, D.D. Liu, K. Fan, G.R. Wang, J. Phys. Chem. C 122 (2018) 10430–10441.
[26] J. Liu, J. Ke, Y. Li, et al., Appl. Catal. B: Environ. 236 (2018) 396–403.
[27] Y.L. Wu, Y.Y. Xu, Y. Zhang, et al., Chin. Chem. Lett. 33 (2022) 2741–2746.
[28] F. Goettmann, A. Fischer, M. Antonietti, A. Thomas, Angew. Chem. Int. Ed. 45 (2006) 4467–4471.
[29] W.J. Ong, L.L. Tan, Y.H. Ng, S.T. Yong, S.P. Chai, Chem. Rev. 116 (2016) 7159–7329.
[30] S.C. Yan, Z.S. Li, Z.G. Zou, Langmuir 25 (2009) 10397–10401.
[31] Q.J. Xiang, J.G. Yu, M. Jaroniec, J. Phys. Chem. C 115 (2011) 7355–7363.
[32] S.W. Cao, J.G. Yu, J. Phys. Chem. Lett. 5 (2014) 2101–2107.
[33] X.F. Li, J.F. Zhang, Y. Huo, et al., Appl. Catal. B: Environ. 280 (2021) 119452.
[34] D.Y. Han, J. Liu, H. Cai, et al., Appl. Surf. Sci. 464 (2019) 577–585.
[35] X.B. Li, B.B. Kang, F. Dong, et al., Nano Energy 81 (2021) 105671.
[36] D.H. Kim, K.J. Yong, Appl. Catal. B: Environ. 282 (2021) 119538.
[37] H.R. Sun, F. Guo, J.J. Pan, et al., Chem. Eng. J. 406 (2021) 126844.
[38] L. Ge, F. Zuo, J.K. Liu, et al., J. Phys. Chem. C 116 (2012) 13708–13714.
[39] G.M. Jiang, J.W. Cao, M. Chen, X.M. Zhang, F. Dong, Appl. Surf. Sci. 458 (2018) 77–85.
[40] X.C. Wang, K. Maeda, A. Thomas, et al., Nat. Mater. 8 (2009) 76–80.
[41] P. Niu, L.L. Zhang, G. Liu, H.M. Cheng, Adv. Funct. Mater. 22 (2012) 4763–4770.
[42] M. Tahir, C.B. Cao, N. Mahmood, et al., ACS Appl. Mater. Interfaces 6 (2014) 1258–1265.
[43] X.J. Bai, L. Wang, R.L. Zong, Y.F. Zhu, J. Phys. Chem. C 117 (2013) 9952–9961.
[44] K. Gu, X.T. Pan, W.W. Wang, et al., Small 14 (2018) 1801812.
[45] X.C. Wang, K. Maeda, X.F. Chen, et al., J. Am. Chem. Soc. 131 (2009) 1680–1681.
[46] X.F. Wu, J.S. Cheng, X.F. Li, Y.H. Li, K.L. Lv, Appl. Surf. Sci. 465 (2019) 1037–1046.
[47] L.B. Jiang, X.Z. Yuan, G.M. Zeng, et al., J. Colloid Interface Sci. 536 (2019) 17–29.
[48] B. Lin, H. Li, H. An, et al., Appl. Catal. B: Environ. 220 (2018) 542–552.
[49] A. Kumar, G. Sharma, A. Kumari, et al., Appl. Catal. B: Environ. 284 (2021) 119808.
[50] Q.H. Liang, X.J. Liu, J.J. Wang, et al., J. Hazard. Mater. 401 (2021) 123355.
[51] P.Y. Kuang, Y.Z. Su, G.F. Chen, et al., Appl. Surf. Sci. 358 (2015) 296–303.
[52] P.F. Xia, B.C. Zhu, J.G. Yu, S.W. Cao, M. Jaroniec, J. Mater. Chem. A 5 (2017) 3230–3238.
[53] M.Q. Qiu, Z.X. Liu, S.Q. Wang, B.W. Hu, Environ. Res. 196 (2021) 110349.
[54] K. Takanabe, K. Kamata, X.C. Wang, et al., Phys. Chem. Chem. Phys. 12 (2010) 13020–13025.
[55] X. Li, H.P. Jiang, C.C. Ma, et al., Appl. Catal. B: Environ. 283 (2021) 119638.
[56] W.Y. Lei, Y. Mi, R.J. Feng, et al., Nano Energy 50 (2018) 552–561.
[57] D. Huang, X.B. Sun, Y.D. Liu, et al., Chin. Chem. Lett. 32 (2021) 2787–2791.
[58] H.R. Sun, L.J. Wang, F. Guo, et al., J. Alloy Compd. 900 (2022) 163410.
[59] P. Zhou, J. Yu, M. Jaroniec, Adv. Mater. 26 (2014) 4920–4935.
[60] L. Shi, Z. Li, K. Marcus, et al., Chem. Commun. 54 (2018) 3747–3750.
[61] J.W. Fu, Q.L. Xu, J.X. Low, C.J. Jiang, J.G. Yu, Appl. Catal. B: Environ. 243 (2019) 556–565.
[62] J.Q. Yan, H. Wu, H. Chen, et al., Appl. Catal. B: Environ. 191 (2016) 130–137.
[63] Q.L. Xu, L.Y. Zhang, J.G. Yu, et al., Mater. Today 21 (2018) 1042–1063.
[64] X. Liu, J. Zhang, Y.M. Dong, et al., New J. Chem. 42 (2018) 12180–12187.
[65] T. Komatsu, T. Nakamura, J. Mater. Chem. 11 (2001) 474–478.
[66] A. Thomas, A. Fischer, F. Goettmann, et al., J. Mater. Chem. 18 (2008) 4893–4908.
[67] Y.S. Jun, W.H. Hong, M. Antonietti, A. Thomas, Adv. Mater. 21 (2009) 4270–4274.
[68] A.K. Geim, Science 324 (2009) 1530–1534.
[69] X.L. Li, G.Y. Zhang, X.D. Bai, et al., Nat. Nanotechnol. 3 (2008) 538–542.
[70] R.Z. Ma, T. Sasaki, Adv. Mater. 22 (2010) 5082–5104.
[71] G.F. Walker, Nature 187 (1960) 312–313.
[72] X.P. Dong, F.X. Cheng, J. Mater. Chem. A 3 (2015) 23642–23652.
[73] K.S. Novoselov, A.K. Geim, S.V. Morozov, et al., Science 306 (2004) 666–669.
[74] Y. Hernandez, V. Nicolosi, M. Lotya, et al., Nat. Nanotechnol. 3 (2008) 563–568.
[75] J.N. Coleman, M. Lotya, A. O'Neill, et al., Science 331 (2011) 568–571.
[76] V. Nicolosi, M. Chhowalla, M.G. Kanatzidis, M.S. Strano, J.N. Coleman, Science 340 (2013) 1226419.
[77] Q.W. Yan, W. Dai, J.Y. Gao, et al., ACS Nano 15 (2021) 6489–6498.
[78] G. Chakraborty, I.H. Park, R. Medishetty, J.J. Vittal, Chem. Rev. 121 (2021) 3751–3891.
[79] S.B. Yang, Y.J. Gong, J.S. Zhang, et al., Adv. Mater. 25 (2013) 2452–2456.
[80] Y.J. Yuan, Z.K. Shen, S.T. Wu, et al., Appl. Catal. B: Environ. 246 (2019) 120–128.
[81] Y. Yin, J.C. Han, X.H. Zhang, et al., RSC Adv. 4 (2014) 32690–32697.
[82] H.P. Liu, S.L. Ma, L. Shao, et al., Appl. Catal. B: Environ. 261 (2020) 118201.
[83] C.Z. Wu, S.Y. Xue, Z.J. Qin, et al., Appl. Catal. B: Environ. 282 (2021) 119557.
[84] Y.Z. Zhang, Z.X. Huang, C.L. Dong, et al., Chem. Eng. J. 431 (2022) 134101.
[85] B.V. Lotsch, M. Döblinger, J. Sehnert, et al., Chemistry 13 (2007) 4969–4980.
[86] L.S. Jiang, J. Li, K. Wang, et al., Appl. Catal. B: Environ. 260 (2020) 118181.
[87] L. Acharya, S.P. Pattnaik, A. Behera, R. Acharya, K. Parida, Inorg. Chem. 60 (2021) 5021–5033.
[88] Z.W. Zhao, Y.J. Sun, Q. Luo, et al., Sci. Rep. 5 (2015) 14643.
[89] W.W. Liu, R.F. Peng, X.P. Ye, J.F. Guo, L.B. Luo, Appl. Surf. Sci. 560 (2021) 150013.
[90] Q.H. Liang, Z. Li, Z.H. Huang, F.Y. Kang, Q.H. Yang, Adv. Funct. Mater. 25 (2015) 6885–6892.
[91] F. Dong, Y.H. Li, Z.Y. Wang, W.K. Ho, Appl. Surf. Sci. 358 (2015) 393–403.
[92] M.L. Zhang, Y. Yang, X.Q. An, et al., J. Hazard. Mater. 424 (2022) 127424.
[93] A. Beyhaqi, S.M.T. Azimi, Z.H. Chen, C. Hu, Q.Y. Zeng, Int. J. Hydrogen Energy 46 (2021) 20547–20559.
[94] S.W. Zhang, H.H. Gao, Y.S. Huang, et al., Environ. Sci.: Nano 5 (2018) 1179–1190.
[95] Y.C. Deng, L. Tang, C.Y. Feng, et al., ACS Appl. Mater. Interfaces 9 (2017) 42816–42828.
[96] Y.Z. Zhang, S.C. Zong, C. Cheng, et al., Appl. Catal. B: Environ. 233 (2018) 80–87.
[97] Y.S. Chen, B. Yang, W.Y. Xie, et al., J. Mater. Res. Technol. 13 (2021) 301–310.
[98] X.L. Liu, Y.H. Guo, P. Wang, et al., Int. J. Hydrogen Energy 46 (2021) 3595–3604.
[99] J. Pan, H.X. Wang, L.A. Xu, et al., Solid State Sci. 129 (2022) 106915.
[100] X.D. Zhang, X. Xie, H. Wang, et al., J. Am. Chem. Soc. 135 (2012) 18–21.
[101] T.M.O. Le, T.H. Lam, T.N. Pham, et al., Polymers (Basel) 10 (2018) 633.
[102] Y.P. Liu, S.J. Shen, Z.G. Li, et al., Mater. Charact. 174 (2021) 111031.
[103] H. Mei, H.W. Shu, M.Y. Lv, W. Liu, X.D. Wang, Microchim. Acta 187 (2020) 159.
[104] Q. Wang, W. Wang, L.L. Zhong, et al., Appl. Catal. B: Environ. 220 (2018) 290–302.
[105] X.F. Zhang, W.J. Du, Q. Li, C.P. Lv, RSC Adv. 12 (2022) 20618–20627.
[106] M.I. Chebanenko, A.A. Lobinsky, V.N. Nevedomskiy, V.I. Popcov, Dalton Trans. 49 (2020) 12088–12097.
[107] D.M. Zhao, J. Chen, C.L. Dong, et al., J. Catal. 352 (2017) 491–497.
[108] X.J. Wang, C. Liu, X.L. Li, et al., Appl. Surf. Sci. 394 (2017) 340–350.
[109] X. Li, Q. Wu, M. Hussain, et al., RSC Adv. 12 (2022) 15378–15384.
[110] H.T. Shin, D.U. Lee, S. Chaudhari, et al., J. Taiwan Inst. Chem. E 132 (2022) 104126.
[111] T.D. Munusamy, S.Y. Chin, M. Tarek, M.M.R. Khan, Int. J. Hydrogen Energy 46 (2021) 30988–30999.
[112] T.V. de Medeiros, A.O. Porto, H.A. Bicalho, et al., J. Mater. Chem. C 9 (2021) 7622–7631.
[113] M.J. Bojdys, N. Severin, J.P. Rabe, et al., Macromol. Rapid Commun. 34 (2013) 850–854.
[114] J. Xu, L.W. Zhang, R. Shi, Y.F. Zhu, J. Mater. Chem. A 1 (2013) 14766–14772.
[115] L. Shi, K. Chang, H.B. Zhang, et al., Small 12 (2016) 4431–4439.
[116] G.N. Li, L. Li, H.Y. Yuan, et al., J. Colloid Interface Sci. 495 (2017) 19–26.
[117] J.F. Wang, J. Chen, P.F. Wang, et al., Appl. Catal. B: Environ. 239 (2018) 578–585.
[118] R.P. Wang, Y. Wang, S.H. Mao, et al., J. Inorg. Organomet. Polym. 31 (2021) 32–42.
[119] A. Mishra, A. Mehta, S. Kainth, S. Basu, J. Mater. Sci. 53 (2018) 13126–13142.
[120] C. Liang, C.G. Niu, H. Guo, et al., Catal. Sci. Technol. 8 (2018) 1161–1175.
[121] Y.Y. Fan, H.M. Chen, D.F. Cui, Z. Fan, C.Y. Xue, Energy Technol. 9 (2021) 2000973.
[122] K.H. Chen, X.W. Wang, Q.Y. Li, et al., Chem. Eng. J. 418 (2021) 129476.
[123] J.P. Wang, Y. Yu, J.Y. Cui, et al., Appl. Catal. B: Environ. 301 (2022) 120814.
[124] J.Z. Jiang, Z.G. Xiong, H.T. Wang, et al., J. Mater. Sci. Technol. 118 (2022) 15–24.
[125] D.V. Thuan, T.L. Nguyen, H.H.P. Thi, et al., Opt. Mater. 123 (2022) 111885.
[126] R.Y. Zhang, S.Y. Niu, J.M. Xiang, et al., Sep. Purif. Technol. 261 (2021) 118258.
[127] Y.Y. Wang, W.J. Jiang, W.J. Luo, X.J. Chen, Y.F. Zhu, Appl. Catal. B: Environ. 237 (2018) 633–640.
[128] H.Y. Wang, R.R. Niu, J.H. Liu, et al., Nano Res. 15 (2022) 6987–6998.
[129] H. Jung, T.T. Pham, E.W. Shin, Appl. Surf. Sci. 458 (2018) 369–381.
[130] K.L. He, J. Xie, M.L. Li, X. Li, Appl. Surf. Sci. 430 (2018) 208–217.
[131] J. Wang, R.H. Pan, Q. Hao, et al., Appl. Surf. Sci. 599 (2022) 153875.
[132] B.L. Dai, Y.Y. Li, J.M. Xu, et al., Appl. Surf. Sci. 592 (2022) 153309.

[133] Z.W. Zhao, K. Dai, J.F. Zhang, G. Dawson, Adv. Sustain. Syst. 7 (2022) 2100498.
[134] A. Mardiroosi, A.R. Mahjoub, H. Fakhri, R. Boukerroub, J. Mol. Struct. 1246 (2021) 131244.
[135] G.L. Xu, H.B. Zhang, J. Wei, et al., ACS Nano 12 (2018) 5333–5340.
[136] J.B. Liu, H.J. Shi, Q. Shen, C.Y. Guo, C.H. Zhao, Green Chem. 19 (2017) 5900–5910.
[137] A. Rajan, B. Neppolian, Appl. Mater. Today 28 (2022) 101524.
[138] Y. Di, X.C. Wang, A. Thomas, M. Antonietti, ChemCatChem 2 (2010) 834–838.
[139] Z.H. Chen, F. Guo, H.R. Sun, Y.X. Shi, W.L. Shi, J. Colloid Interface Sci. 607 (2021) 1391–1401.
[140] T.Y. Ren, Y.P. Dang, Y. Xiao, et al., Inorg. Chem. Commun. 123 (2021) 108367.
[141] J.W. Zhou, F.F. Duo, C.Y. Jia, et al., Environ. Eng. Sci. 38 (2021) 1098–1107.
[142] T. Tong, B.C. Zhu, C.J. Jiang, B. Cheng, J.G. Yu, Appl. Surf. Sci. 433 (2018) 1175–1183.
[143] S.J. Wang, Y.X. Feng, M.A. Yu, Q. Wan, S. Lin, ACS Appl. Mater. Interfaces 9 (2017) 33267–33273.
[144] X.L. Zhang, X.X. Zhang, J.D. Li, et al., Appl. Catal. B: Environ. 237 (2018) 50–58.
[145] W. Liu, Y.Y. Li, F.Y. Liu, et al., Water Res. 151 (2019) 8–19.
[146] Z.Y. Shi, L. Rao, P.F. Wang, L.X. Zhang, Chemosphere 308 (2022) 136257.
[147] Z.Y. Shi, L. Rao, P.F. Wang, L.X. Zhang, Environ. Sci. Pollut. Res. 29 (2022) 83981–83992.
[148] M. Karimi-Nazarabad, E.K. Goharshadi, R. Mehrkhah, M. Davardoostmanesh, Sep. Purif. Technol. 279 (2021) 119788.
[149] H.J. He, L.H. Huang, Z.J. Zhong, S.Z. Tan, Appl. Surf. Sci. 441 (2018) 285–294.
[150] D. Liu, J. Yao, S.T. Chen, et al., Appl. Catal. B: Environ. 318 (2022) 121822.
[151] F.G. Hu, S.P. Sun, H.L. Xu, et al., J. Phys. Chem. Solids 156 (2021) 110181.
[152] X.J. Chen, J. Wang, Y.Q. Chai, Z.J. Zhang, Y.F. Zhu, Adv. Mater. 33 (2021) 2007479.
[153] P. Sarkar, S.R.D. De, S. Neogi, Appl. Catal. B: Environ. 307 (2022) 121165.
[154] J.E. Du, S.L. Ma, N. Zhang, et al., Colloid. Surf. A 654 (2022) 130094.
[155] W.L. Shi, C. Liu, M.Y. Li, et al., J. Hazard. Mater. 389 (2020) 121907.
[156] H.F. Xu, S.J. Liang, X. Zhu, et al., Biosens. Bioelectron. 92 (2017) 695–701.
[157] Q. Qiao, W.Q. Huang, Y.Y. Li, et al., J. Mater. Sci. 53 (2018) 15882–15894.
[158] W.N. Xing, G. Chen, C.M. Li, et al., Nanoscale 10 (2018) 5239–5245.
[159] Y.Y. Liu, Y. Zhang, L. Shi, Colloid Surf. A 641 (2022) 128577.
[160] M.Y. Cao, K. Wang, I. Tudela, X.F. Fan, Appl. Surf. Sci. 536 (2021) 147784.
[161] Y. Ding, S. Maitra, C.H. Wang, et al., J. Energy Chem. 70 (2022) 236–247.
[162] L. Deng, J.J. Sun, J. Sun, et al., Appl. Surf. Sci. 597 (2022) 153586.
[163] B. Yang, X.L. Li, Q. Zhang, et al., Appl. Catal. B: Environ. 314 (2022) 121521.
[164] S. Mao, C. Liu, Y. Wu, M.Z. Xia, F.Y. Wang, Chemosphere 291 (2022) 133039.
[165] J.C. Wang, Y.X. Huo, F.D. Feng, et al., Appl. Surf. Sci. 537 (2021) 148014.
[166] X.A. Dong, J.Y. Li, Q. Xing, Y. Zhou, H.W. Huang, Appl. Catal. B: Environ. 232 (2018) 69–76.
[167] C.H. Choi, L.H. Lin, S.J. Gim, et al., ACS Catal. 8 (2018) 4241–4256.
[168] C.C. Dong, Z.Y. Ma, R.T. Qie, et al., Appl. Catal. B: Environ. 217 (2017) 629–636.
[169] S.H. Cao, B. Fan, Y.C. Feng, et al., Chem. Eng. J. 353 (2018) 147–156.
[170] G.H. Dong, D.L. Jacobs, L. Zang, C.Y. Wang, Appl. Catal. B: Environ. 218 (2017) 515–524.
[171] Q.C. Li, Y.W. Tong, Y.B. Zeng, X.K. Gu, M.Y. Ding, Chem. Eng. J. 450 (2022) 138010.
[172] F.P. Meng, W.J. Tian, Z.H. Tian, et al., Sci. Total Environ. 851 (2022) 158360.
[173] H.W. Huang, K. Xiao, N. Tian, et al., J. Mater. Chem. A 5 (2017) 17452–17463.
[174] Z.Q. Jiang, Y.R. Shen, Y.J. You, Molecules 27 (2022) 6054.
[175] T.T. Li, S.L. Wang, L. Li, et al., J. Colloid Interface Sci. 628 (2022) 214–221.
[176] Q. Liu, X.L. Wang, Q. Yang, Z.G. Zhang, X.M. Fang, Appl. Surf. Sci. 450 (2018) 46–56.
[177] S.W. Cao, J.X. Low, J.G. Yu, M. Jaroniec, Adv. Mater. 27 (2015) 2150–2176.
[178] J.J. Yi, T. Fei, L. Li, et al., Appl. Catal. B: Environ. 281 (2021) 119475.
[179] A. Majumdar, U. Ghosh, A. Pal, et al., J. Colloid Interface Sci. 584 (2021) 320–331.
[180] C. Murugan, K. Ranjithkumar, A. Pandikumar, et al., J. Colloid Interface Sci. 602 (2021) 437–451.
[181] H.J. Li, Y. Zhou, W.G. Tu, J.H. Ye, Z.G. Zou, Adv. Funct. Mater. 25 (2015) 998–1013.
[182] W.K. Jo, N.C.S. Selvam, Chem. Eng. J. 317 (2017) 913–924.
[183] M.Q. Wu, T. Ding, Y.T. Wang, et al., Catal. Today 355 (2020) 311–318.
[184] Z.X. Liu, Y.D. Liu, X.B. Sun, et al., Chem. Eng. J. 433 (2022) 133604.
[185] I. Hong, Y.A. Chen, Y.J. Hsu, K.J. Yong, ACS Appl. Mater. Interfaces 13 (2021) 52670–52680.
[186] P. Wen, Y.H. Sun, H. Li, et al., Appl. Catal. B: Environ. 263 (2020) 118180.
[187] J.G. Yu, S.H. Wang, J.X. Low, W. Xiao, Phys. Chem. Chem. Phys. 15 (2013) 16883–16890.
[188] G.X. Li, Y.D. Cai, X.D. Wang, et al., Chem. Phys. 559 (2022) 111558.
[189] H. Zhang, J. He, P. Wu, W. Jiang, J. Environ. Chem. Eng. 10 (2022) 107804.
[190] T. Feng, J.Y. Jin, Y.R. Cao, et al., Int. J. Hydrogen Energy 47 (2022) 5999–6010.
[191] N.K. Ding, B. Chen, L. Zhou, et al., Chin. Chem. Lett. 33 (2022) 3797–3801.
[192] M.X. Zhang, H.X. Du, J. Ji, et al., Molecules 26 (2021) 2062.
[193] K. Wang, G.K. Zhang, J. Li, Y. Li, X.Y. Wu, ACS Appl. Mater. Interfaces 9 (2017) 43704–43715.
[194] N. Nie, L.Y. Zhang, J.W. Fu, B. Cheng, J.G. Yu, Appl. Surf. Sci. 441 (2018) 12–22.
[195] X.W. Liu, J. Chen, L.F. Yang, et al., J. Phys. Chem. Solids 160 (2021) 110339.
[196] X.F. Zhang, X.B. Jia, P.Z. Duan, et al., Colloid Surf. A 608 (2021) 125580.
[197] Q. Ye, M. Yang, W. Li, et al., Environ. Sci. Pollut. Res. 29 (2022) 58762–58772.
[198] P. Ke, D.L. Zeng, J.W. Cui, X. Li, Y. Chen, Catalysts 12 (2022) 247.
[199] X.L. Zhu, C.L. Duan, W.Z. Wang, G.X. Xin, J.L. Song, Mater. Lett. 317 (2022) 132045.
[200] X.D. Yang, J. Duan, X. Zhang, et al., Chin. Chem. Lett. 33 (2022) 3792–3796.
[201] D.T. Dung, N.V. Hiep, M.B. Nguyen, V.D. Thao, N.N. Huy, Korean J. Chem. Eng. 38 (2021) 2034–2046.
[202] M. Li, Q.H. Li, M.W. Xu, et al., Carbon 184 (2021) 479–491.
[203] A. Hagghi, N. Dalali, M.M. Abolghasemi, et al., Sep. Sci. Technol. 56 (2021) 2398–2406.
[204] D.D. Zhang, J.J. Qi, H.D. Ji, et al., Chem. Eng. J. 400 (2020) 125918.
[205] L.M. Zhao, L.J. Guo, Y.L. Tang, J.F. Zhou, B. Shi, Ind. Eng. Chem. Res. 60 (2021) 13594–13603.
[206] M.Y. Xu, X.X. Zhao, H.P. Jiang, S.T. Chen, P.W. Huo, J. Environ. Chem. Eng. 9 (2021) 106469.
[207] Z.L. Tang, C.J. Wang, W.J. He, et al., Chin. Chem. Lett. 33 (2022) 939–942.
[208] X.X. Zhao, M. Gao, Q. Liu, et al., Sustain. Energy Fuels 6 (2022) 3768–3777.
[209] Z.W. Zhao, Y.J. Sun, F. Dong, Nanoscale 7 (2015) 15–37.
[210] Z.L. Jin, Y.B. Li, X.Q. Hao, Acta Phys. Chim. Sin. 37 (2021) 1912033.
[211] Y.X. Wang, F.T. He, L. Chen, et al., Chin. Chem. Lett. 31 (2020) 2668–2672.
[212] W. Tahir, T.Y. Cheang, J.H. Li, et al., Catal. Sci. Technol. 12 (2022) 2023–2029.
[213] W. Zhao, Y.J. Li, P.S. Zhao, et al., Chem. Eng. J. 405 (2021) 126555.
[214] C. Cheng, L.H. Mao, J.W. Shi, et al., J. Mater. Chem. A 9 (2021) 12299–12306.
[215] J. Jia, W.J. Sun, Q.Q. Zhang, et al., Appl. Catal. B: Environ. 261 (2020) 118249.
[216] X.X. He, H.Y. Shang, C. Wang, et al., Chin. Chem. Lett. 32 (2021) 3377–3381.
[217] I. Camussi, B. Mannucci, A. Speltini, et al., ACS Sustain. Chem. Eng. 7 (2019) 8176–8182.
[218] Y. Li, Y.N. Li, S.L. Ma, et al., J. Hazard. Mater. 338 (2017) 33–46.
[219] Q.D. Le, P.N. Ngoc, H.T. Huu, et al., Chem. Phys. Lett. 796 (2022) 139550.
[220] Z.P. Li, W.X. Dong, X.Y. Du, G.M. Wen, X.J. Fan, Microchem. J. 152 (2020) 104259.
[221] E. Dhandapani, S. Prabhu, N. Duraisamy, R. Ramesh, J. Energy Storage 44 (2021) 103360.
[222] F. Goudarzy, J. Zolgharnein, J.B. Ghasemi, Inorg. Chem. Commun. 141 (2022) 109512.
[223] K. Radhakrishnan, S. Sivanesan, P. Panneerselvam, J. Photochem. Photobiol. A 389 (2020) 112204.
[224] X.J. Liu, Q.E. Wang, J. Chen, X. Chen, W.S. Yang, Talanta 221 (2021) 121379.